Available online at www.eccomasproceedia.org
Eccomas Proceedia COMPDYN (2023) 1605-1614

ECCOMAS
Proceedia

COMPDYN 2023
9th ECCOMAS Thematic Conference on
Computational Methods in Structural Dynamics and Earthquake Engineering
M. Papadrakakis, M. Fragiadakis (eds.)
Athens, Greece, 12-14 June 2023

HETEROGENEOUS LIMIT ANALYSIS FOR MASONRY ARCH BRIDGES WITH FULL MODELING OF BACKFILL

Yiwei Hua[1] **and Gabriele Milani**[2]

[1] Politecnico di Milano, Department of Architecture, Built Environment and Construction Engineering
Piazza Leonardo da Vinci 32, 20133 Milan, Italy
e-mail: yiwei.hua@polimi.it

[2] Politecnico di Milano, Department of Architecture, Built Environment and Construction Engineering
Piazza Leonardo da Vinci 32, 20133 Milan, Italy
e-mail: gabriele.milani@polimi.it

Abstract

Masonry arch bridges are widespread architectural heritages worldwide but are vulnerable to many disasters, such as floods and earthquakes. Understanding the failure mechanism of these bridges is very important. Recent works regarding the collapse analysis of masonry arch bridges almost neglected the backfill, whose absence will lead to inaccuracy in numerical simulation. This contribution discusses how to model the backfill when analyzing the collapse of masonry arch bridges in heterogeneous limit analysis. In this paper, the collapse of the bridge with triangular, random Voronoi, and centroid Voronoi mesh of the backfill is first compared. For such purpose, we in a prior extend the formulation of standard heterogeneous limit analysis to be applicable to arbitrary polygon elements. Then, we compare the collapse performance of the bridge employing an associated or non-associated sliding model at the interface of the backfill. The results show that although the employment of polygon elements for backfill can produce a more realistic crack propagation, it may also lead to severe locking problems, resulting in an overestimated load prediction. Besides, we would recommend employing a non-associated flow rule for a conservative prediction of collapse load (especially when using a polygon mesh).

Keywords: Masonry arch bridges, Backfill, Limit analysis, Associated sliding, Non-associated sliding, Polygon mesh.

ISSN:2623-3347 Published by Eccomas Proceedia.
Peer-review under responsibility of the organizing committee of COMPDYN 2023.
doi: 10.7712/120123.10505.20314

1 INTRODUCTION

Masonry arch bridges are one of the most widespread typologies in worldwide architectural heritages. The collapse analysis of these bridges is a complex problem in the numerical field due to the involvement of multiple materials. Besides the stone-like part (e.g. arch or spandrel), the backfill on the ring presents completely different properties from the stone. The presence of the backfill has a positive influence on the ultimate load of the bridges because it can prevent the movement of the bricks when the bridge turns into a mechanism, and such effects have been experimentally proven [1, 2]. Therefore, how to model the backfill when analyzing the collapse of these bridges should be a great concern to investigate.

Rigid block limit analysis is one of the powerful approaches that can quickly predict the collapse of block structures. This approach has been gaining popularity due to the recent boom of Computational Operational Research (e.g. [3−6]). Backfill, however, was not precisely taken into account in these numerical works. Some researchers attempted to engage backfill when analyzing the failure of masonry arch bridges [7−11]. In these contributions, they proposed a limit-analysis-based formulation, with a triangular discretization of the backfill. Nevertheless, such discretization for backfill can only produce straight crack propagation, which should deviate from reality. On the other hand, sliding behavior among the backfill elements has not been precisely considered. In these studies, the employed sliding model for the backfill interface was the associated flow rule (see [7, 8]). Such a model will lead to a large separation (dilation) at the contact joint and thus may give rise to an incorrect collapse mechanism and overestimated collapse load (see [12, 13]). The real sliding behavior for the backfill-to-backfill interface should be more closed to a non-associated sliding with zero-dilation angle [14].

In this paper, we discuss the modeling of the backfill in the limit analysis of masonry arch bridges. The formulation for the associated limit analysis with arbitrary polygon elements is first developed, then we extend it to tackling the non-associated sliding problem. Utilizing the above approach, we investigate the influence of different mesh shapes for the backfill on the collapse performance, with consideration of three types of discretization: a) triangular mesh; b) random Voronoi mesh; c) centroid Voronoi mesh. Here, Prestwood bridge is taken as a benchmark. The collapse predicted by associated and non-associated formulations is also compared. Based on these results, some suggestions for modeling the backfill when performing a limit analysis are concluded.

2 METHODOLOGY

Many contributions have established the associated formulation of limit analysis for triangular or quadrilateral blocks [15, 16]. In this section, to include also polygon elements, we first investigate the equilibrium and compatibility conditions for these elements.

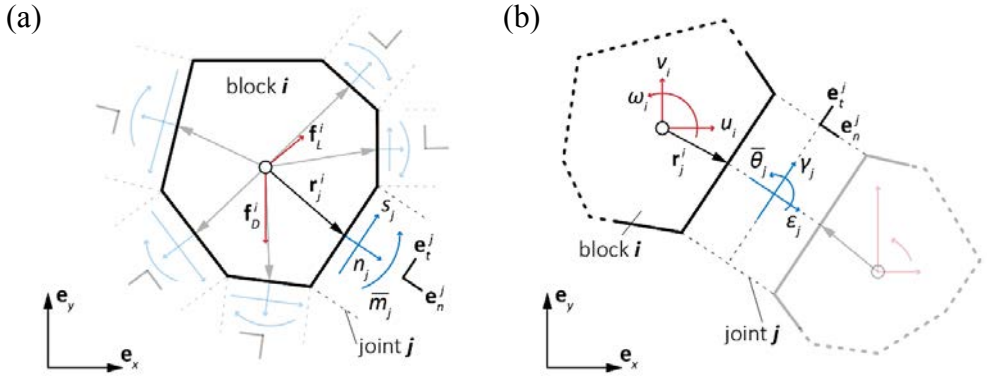

Figure 1: (a) equilibrium condition and (b) geometric compatibility condition for polygon element.

Considering a polygon block i, the equilibrium condition between the interfacial resultant and centroid-acting force (Figure 1a) can be written as Eq. (1). J_i represent the set of the joint index associated with block i. Correspondingly, from point of view of kinematics (Figure 1b), we can calculate the velocity jumps at each interface j from the centroid velocities by Eq. (2). I_j represent the set of the block index associated with joint j. sgn (x) here is the sign function.

$$\begin{aligned}
&-\mathrm{sgn}(\mathbf{r}_j^i\mathbf{e}_n^j)\sum_{j\in J_i}\left(n_j\mathbf{e}_n^j\mathbf{e}_x+s_j\mathbf{e}_t^j\mathbf{e}_x\right)=\alpha F_{Lx}^i+F_{Dx}^i\\
&-\mathrm{sgn}(\mathbf{r}_j^i\mathbf{e}_n^j)\sum_{j\in J_i}\left(n_j\mathbf{e}_n^j\mathbf{e}_y+s_j\mathbf{e}_t^j\mathbf{e}_y\right)=\alpha F_{Ly}^i+F_{Dy}^i\\
&-\mathrm{sgn}(\mathbf{r}_j^i\mathbf{e}_n^j)\sum_{j\in J_i}\left(-n_j\mathbf{r}_j^i\mathbf{e}_t^j+s_j\mathbf{r}_j^i\mathbf{e}_n^j+\bar{m}_j\right)=\alpha M_L^i+M_D^i
\end{aligned}\tag{1}$$

$$\begin{aligned}
\varepsilon_j&=\mathrm{sgn}(\mathbf{r}_j^i\mathbf{e}_n^j)\sum_{i\in I_j}\left(\mathbf{e}_x\mathbf{e}_n^ju_i+\mathbf{e}_y\mathbf{e}_n^jv_i-\mathbf{r}_j^i\mathbf{e}_t^j\omega_i\right)\\
\gamma_j&=\mathrm{sgn}(\mathbf{r}_j^i\mathbf{e}_n^j)\sum_{i\in I_j}\left(\mathbf{e}_x\mathbf{e}_t^ju_i+\mathbf{e}_y\mathbf{e}_t^jv_i+\mathbf{r}_j^i\mathbf{e}_n^j\omega_i\right)\\
\bar{\theta}_j&=\mathrm{sgn}(\mathbf{r}_j^i\mathbf{e}_n^j)\sum_{i\in I_j}\omega_i
\end{aligned}\tag{2}$$

These two formulations can be cast into a matrix form (Eqs. (3) and (4)).

$$\sum_{j\in J_i}\mathrm{sgn}\left(\mathbf{r}_j^i\mathbf{e}_n^j\right)\mathbf{A}_j^i\mathbf{x}_j=\alpha\mathbf{f}_L^i+\mathbf{f}_D^i,\ J_i=\{j\mid \text{joint } j \text{ is associated with block } i\}\tag{3}$$

$$\sum_{i\in I_j}\mathrm{sgn}\left(\mathbf{r}_j^i\mathbf{e}_n^j\right)\left(\mathbf{A}_j^i\right)^T\mathbf{u}_i=\mathbf{q}_j,\ I_j=\{i\mid \text{block } i \text{ is associated with joint } j\}\tag{4}$$

Where:

$$\mathbf{A}_j^i=\begin{bmatrix}\mathbf{e}_n^j\mathbf{e}_x & \mathbf{e}_t^j\mathbf{e}_x & 0\\ \mathbf{e}_n^j\mathbf{e}_y & \mathbf{e}_t^j\mathbf{e}_y & 0\\ -\mathbf{e}_t^j\mathbf{r}_j^i & \mathbf{e}_n^j\mathbf{r}_j^i & 1\end{bmatrix},\ \mathbf{x}_j=\begin{bmatrix}n_j\\ s_j\\ \bar{m}_j\end{bmatrix},\ \mathbf{u}_i=\begin{bmatrix}u_i\\ v_i\\ \omega_i\end{bmatrix},\ \mathbf{q}_j=\begin{bmatrix}\varepsilon_j\\ \gamma_j\\ \bar{\theta}_j\end{bmatrix}\tag{5}$$

Note that here all the components in the matrix $\mathbf{A}_j^i$ completely depend on the geometry of the blocks. Matrix $\mathbf{A}_j^i$ project the joint resultants $\mathbf{x}_j$ onto the global coordinate frame regarding the centroid of the blocks. Matrix $\left(\mathbf{A}_j^i\right)^T$ transforms the centroid velocities $\mathbf{u}_i$ to the interfacial discontinuous variable $\mathbf{q}_j$. As we can see, similar to the case for triangular or quadrilateral blocks, the coefficient matrix for the equilibrium and compatibility condition is a transpose of each other. Vector $\mathbf{f}_L^i$ and $\mathbf{f}_D^i$ contain the components of live and dead load. In the vertical loading case, we can assign them as Eq. (6). W_i here is the weight of the block i.

$$\mathbf{f}_L^i=\begin{bmatrix}0\\ -1\\ 0\end{bmatrix},\ \mathbf{f}_D^i=\begin{bmatrix}0\\ -W_i\\ 0\end{bmatrix}\tag{6}$$

Collecting the Eqs. (3) and (4) for all the elements, we can get global equilibrium and compatibility conditions for arbitrary polygon blocks. The form is in line with the one in rigid block limit analysis for triangular or quadrilateral elements. The optimization formulation for Lower Bound (LB) and Upper Bound (UB) problems can then be written as Eqs. (7) and (8).

$$\begin{aligned} &\text{maximize} && \alpha \\ &\text{subject to} && \mathbf{A}\mathbf{x} = \alpha\mathbf{f}_L + \mathbf{f}_D \\ & && \mathbf{N}\mathbf{x} - \mathbf{c}_0 = \mathbf{z} \\ & && \mathbf{z} \le 0 \end{aligned} \tag{7}$$

$$\begin{aligned} &\text{minimize} && -\mathbf{f}_D^T\mathbf{u} + \mathbf{c}_0^T\mathbf{p} \\ &\text{subject to} && \mathbf{f}_L^T\mathbf{u} = 1 \\ & && \mathbf{A}^T\mathbf{u} = \mathbf{q} \\ & && \mathbf{N}^T\mathbf{p} = \mathbf{q}, \mathbf{p} \ge 0 \end{aligned} \tag{8}$$

Besides the equilibrium and compatibility conditions, we use Mohr-Coulomb friction to model the interfacial behavior (the second condition in Eq. (7)). This model defines a limit surface for the interfacial resultants (Figure 2). Any force state that reaches the edges will imply separation or sliding at the joint. The corresponding flow rule (the third condition in Eq. (8)) is associated, which means that the possible interfacial velocity resultants should be orthogonal to the limit surface. In that case, Eqs. (7) and (8) become a pair of dual Linear Programming (LP) problems, which should always give a consistent optimal solution. More information can refer to [16].

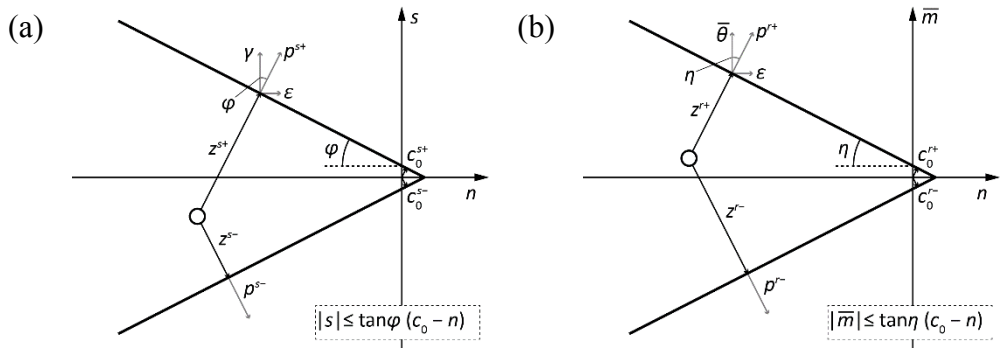

Figure 2: Failure surfaces for the interfaces: (a) normal force vs. shear force; (b) normal force vs. moment.

Although the problem will be robust to be solved once employing the associated flow, such a model will give rise to a large separation at the joint. A more realistic model of the interfacial sliding for the backfill should be non-associated and zero-dilation. However, such a non-associativity will make the optimization problem non-convex and will thus increase the complexity when searching for the solution. We use the Sequential Linear Programming (SLP) procedure to solve this problem [13]. This procedure sequentially solves a series of associated limit analysis problems through LP procedure. During the Iteration, the dilation angles for the discontinuous velocity will be gradually reduced while the constraints for the interfacial resultants remain. Finally, the solution will eventually converge to a non-associated one.

3 CASE STUDY: PRESTWOOD BRIDGE

Implementing the proposed approach, we analyze the collapse of "Prestwood Bridge" as a case study. The span of the bridge is 6550 mm, with a rise of 1428 mm. The thickness of the arch ring is 220 mm. Detailed geometric characteristic of this bridge is shown in Figure 3 (referring to [7]). The boundary at the side and bottom of the backfill as well as the springer are all unilateral contact conditions. The load pattern considered here is a pressure with a width of 300 mm, acting at the 1/4 span of the bridge. The material properties of the elements and the

interfaces are given in Table 1. Note that here the cohesion for the brick-to-backfill and brick-to-brick interfaces are almost neglected (assigned with a very trivial value 10^{-6} MPa).

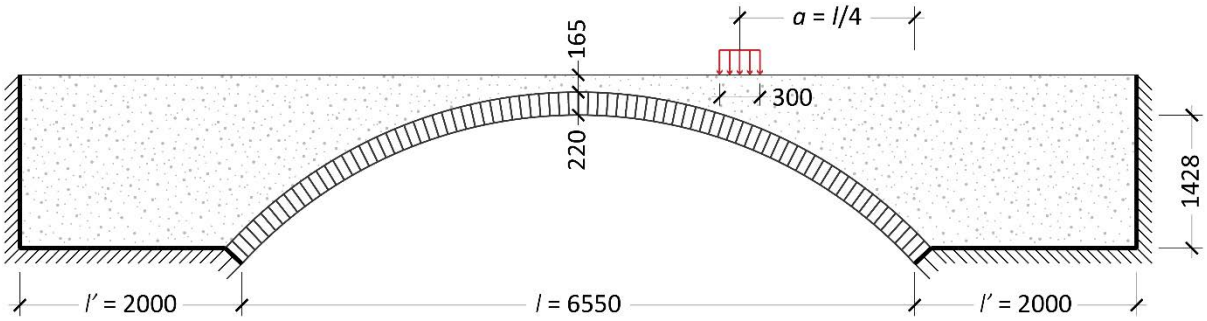

Figure 3: Geometry of the Prestwood Bridge (referring to [7]).

	Elements		Interfaces		
	brick	backfill	Brick-to-brick	Brick-to-backfill	Backfill-to-backfill
Density ρ [kg/m^3]	15	19	-	-	-
Frictional angle φ [°]	-	-	37	37	37
Cohesion c [MPa]	-	-	10^{-6}	10^{-6}	10^{-3}

Table 1: Material parameters for the elements and interfaces.

Taking this bridge as a benchmark, we compare the collapse with the employment of different discretization (triangular and polygon mesh) and interfacial sliding models (associated and non-associated sliding). As mentioned in the methodology, associated and non-associated sliding problems are solved through LP and SLP procedures, respectively.

3.1 Rigid triangular mesh for backfill

The triangular mesh for the backfill region is presented in Figure 4. The arch ring is discretized as 80 rigid blocks, based on the real bond pattern of the bridge. Triangular mesh is generated through a MATLAB-based package "MESH2D" [17]. The typical size of the element is about 131 mm. The total amount of the element for backfill is 1605.

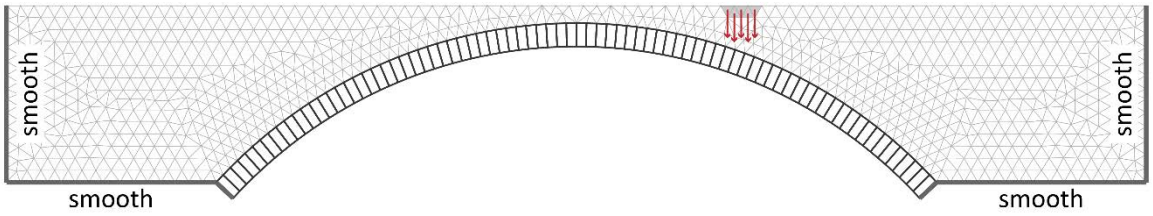

Figure 4: Mesh, load, and boundary condition: triangular mesh for the backfill.

The collapse of the bridge predicted by the associated formulation is shown in Figure 5a. The mechanism for the arch ring is similar to a 4-hinge mechanism. Two extrados hinges occur below the loading area and the distance between these two extrados hinges is larger than the width of the pressure acting on the surface of the backfill. This indicates that the dispersion of the pressure takes place in this region. Other hinges locate near the middle span and two springers of the bridge, which is basically consistent with the standard 4-hinge mechanism. The

backfill at the right side moves downward and the left rises due to the arch ring extrusion. Note that the vertical movement of the left part is greater than the right, especially for the element at the top layer, and we also observe large separations exhibited at the top of the backfill. The backfill cracks from the surface to the bottom on the right side with comparatively small separations. Most of the cracks in the backfill are straight.

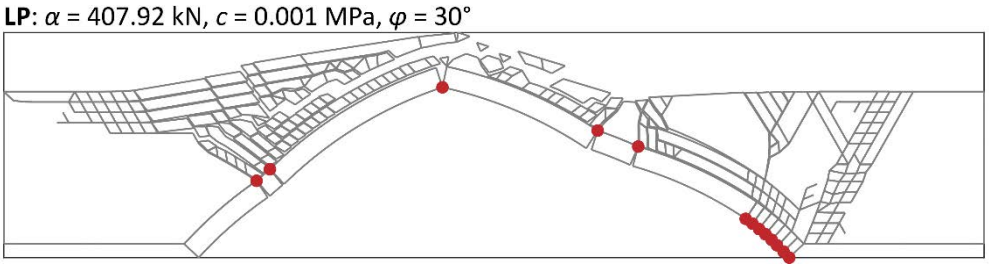

(a) Associated flow

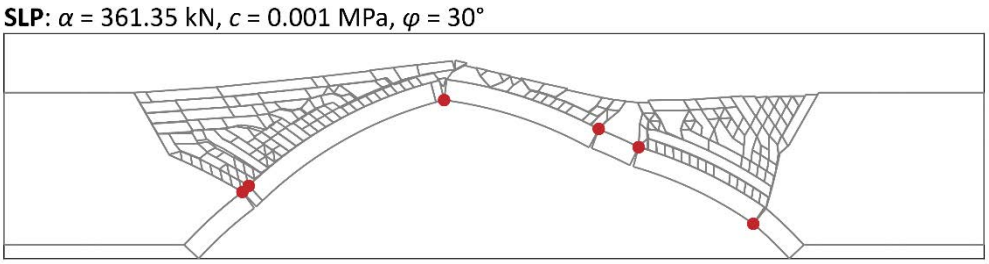

(b) Non-associated flow

Figure 5: Collapse results of the bridge: triangular mesh for the backfill

Compared with the associated one, the predicted mechanism for the arch ring is very similar (Figure 5b). Only the number of hinges at the right springer decreases. The movement of the backfill is roughly in line with the associated one while the cracking area is significantly reduced (especially for the left side). Due to employing the zero-dilation angle, no obvious separation is presented in the backfill. Regarding the collapse load, the non-associated prediction is 9.85% lower than the associated one, indicating that the associated formulation will overestimate the ultimate load in this case.

3.2 Rigid polygon mesh for backfill

Now Let us proceed to investigate the collapse of the bridge where the backfill is discretized by the polygon elements. In this analysis, polygon mesh is produced based on Voronoi tessellation. Two types of Voronoi mesh for the backfill are considered: a) random Voronoi mesh, where the shape of the polygon is more random (Figure 6a); b) centroid Voronoi mesh, where the shape of the polygon is more regular (Figure 6b). Both these two meshes are generated through an open-source code "lloydsAlgorithm" [18]. The total amount of the element in these two cases is 1159. The arrangement of the bricks is the same as the one in the previous triangular-element case.

Employing the random Voronoi mesh, the associated formulation predicts a very different mechanism (Figure 7a), compared with that in the triangular-meshed case. Sliding happens in the collapse mechanism of the arch (at two springers). Excessive cracks spread in the left part of the backfill, with also the occurrence of large separations among the elements. Using the non-associated formulation can reduce the cracking and the separation within the backfill region (Figure 7b). The movement of the backfill is almost consistent with the one in the

triangular-meshed case. Note that the predicted crack propagation in the backfill is zig-zag, which should be more realistic. However, the collapse load predicted by the associated formulation is extremely overestimated when using the random Voronoi mesh (about 10 times the associated solution in the triangular-meshed case), which should be attributed to the locking of the rigid polygon element. Such overestimation will drop when using the non-associated sliding while the predicted load remains 64.2% higher than that given in the triangular-element case. In conclusion, although the consideration of the non-associated sliding can relieve the locking among the random Voronoi elements to some extent, it still exists.

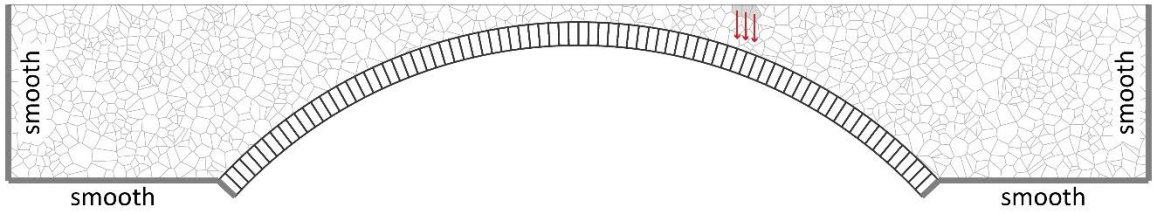

(a) Random Voronoi mesh

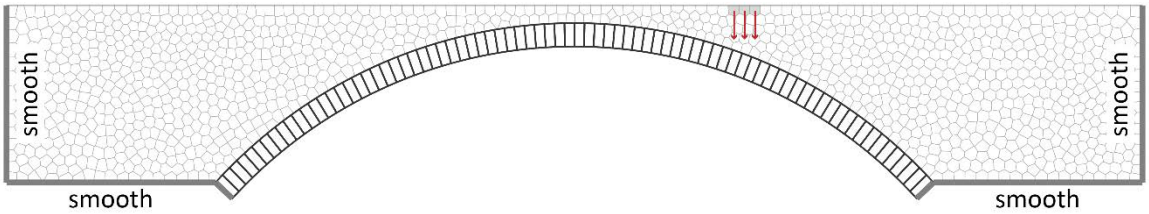

(b) Centroid Voronoi mesh

Figure 6: Mesh, load, and boundary condition: polygon mesh for the backfill.

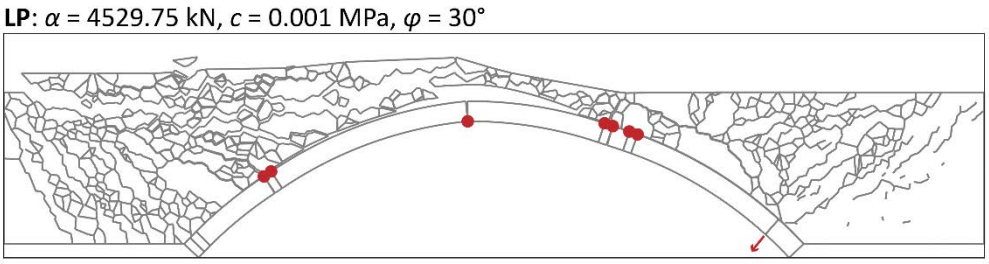

(a) Associated flow

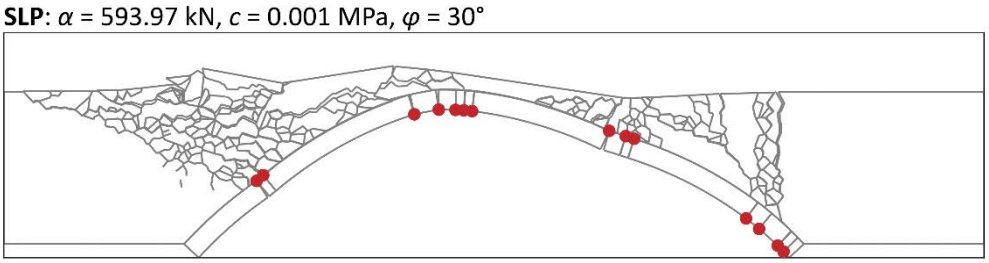

(b) Non-associated flow

Figure 7: Collapse results of the bridge: random Voronoi mesh for the backfill.

Such a locking phenomenon becomes even more severe when applying a centroid Voronoi mesh. Both associated and non-associated formulations produce a very large collapse load

(Figure 8). In this case, the collapse load predicted by the non-associated formulation is even higher than the associated one (compare Figures 8a and 8b). This indicates that considering non-associated sliding cannot reduce the locking phenomenon, which may even go worse during the SLP iteration. The collapse mechanisms of the bridge predicted by these two formulations also significantly deviate from intuition (see Figure 8).

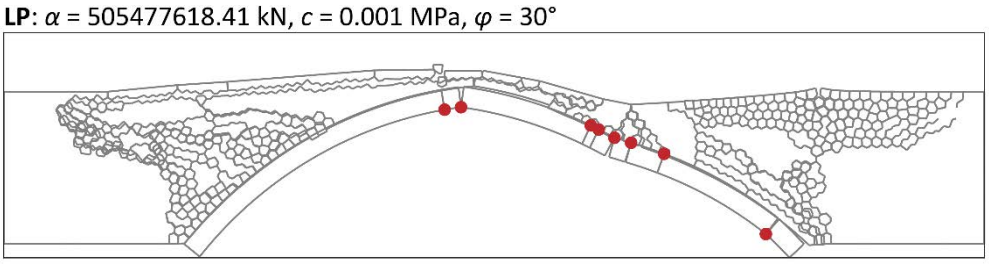

(a) Associated flow

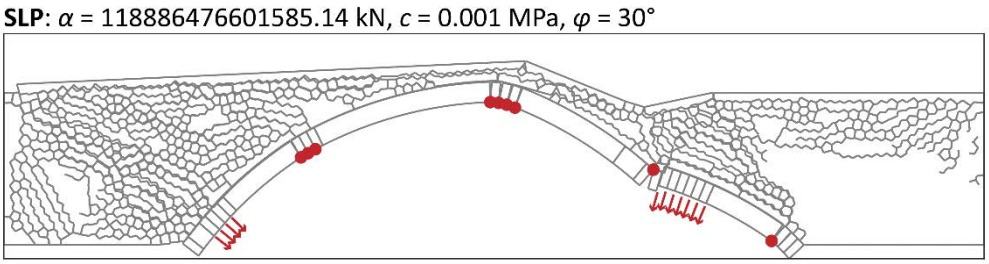

(b) Non-associated flow

Figure 8: Collapse results of the bridge: centroid Voronoi mesh for the backfill.

4 CONCLUSIONS

This paper has investigated the collapse of the masonry arch bridges with different meshes and interfacial sliding models for the backfill through limit analysis. For this purpose, we first extended the associated and non-associated limit analysis to be also applicable to arbitrary polygon elements. Collapse analysis of Prestwood Bridge was carried out as a benchmark to compare the aforementioned aspects. Specifically, we compared the collapse performance of the bridge employing triangular/polygon mesh and associated/non-associated interfacial sliding for backfill. The main conclusions are drawn as follows:

- In the 1/4-span-loading case, the arch collapses as a 4-hinge mechanism in general. The backfill at the loading side moves downward while another side moves upwards due to the passive extrusion of the arch. Dispersion of the surface pressure in the backfill is also observed.
- Collapse mechanism of the bridge with triangular mesh for the backfill is in line with the intuition while the produced cracks among the backfill are straight. Employment of polygon elements will suffer from the locking phenomenon to some extent, resulting in an overestimated collapse load. However, the predicted zig-zag crack propagation among the backfill should be more realistic.
- According to our research, when using the rigid polygon elements, we would recommend the random Voronoi mesh, because the overestimation of the load is comparatively low in this case.

- Generally, using the non-associated flow rule can reduce large separations among the backfill and thus give rise to a safer collapse load. We would recommend using the non-associated flow rule, especially when using polygon mesh, because the overestimation of the associated formulation, in this case, may be very large.
- Future work will concern how to reduce the locking phenomenon when using the polygon elements. Further calibration of the material parameters for a more precise prediction of the collapse load will also be carried out.

REFERENCES

[1] J. Page. Load Tests to Collapse on Two Arch Bridges at Preston, Shropshire and Prestwood, Staffordshire. *Res. Rep. - Transp. Road Res. Lab.* 1987.

[2] R. Royles, A. W. Hendry. Model tests on masonry arches. *Proc. - Inst. Civ. Eng. Part 2. Res. theory*. **91**, 299–321,1991.

[3] N. Makris, H. Alexakis. The effect of stereotomy on the shape of the thrust-line and the minimum thickness of semicircular masonry arches. *Arch. Appl. Mech.*, **83**, 1511–1533, 2013.

[4] A. Chiozzi, N. Grillanda, G. Milani, A. Tralli. UB-ALMANAC: An adaptive limit analysis NURBS-based program for the automatic assessment of partial failure mechanisms in masonry churches. *Eng. Fail. Anal.*, **85**, 201–220, 2018.

[5] A. Chiozzi, M. Malagù, A. Tralli, A. Cazzani. ArchNURBS: NURBS-Based Tool for the Structural Safety Assessment of Masonry Arches in MATLAB. *J. Comput. Civ. Eng.*, **30**, 4015010, 2016.

[6] N. Grillanda, M. Valente, G. Milani. ANUB-Aggregates: a fully automatic NURBS-based software for advanced local failure analyses of historical masonry aggregates. *Bull. Earthq. Eng.*, **18**, 3935–3961, 2020.

[7] A. Cavicchi, L. Gambarotta. Two-dimensional finite element upper bound limit analysis of masonry bridges. *Comput. Struct.*, **84**, 2316–2328, 2006.

[8] A. Cavicchi, L. Gambarotta. Collapse analysis of masonry bridges taking into account arch-fill interaction. *Eng. Struct.*, **27**, 605–615, 2005.

[9] T. Papa, N. Grillanda, G. Milani. Three-dimensional adaptive limit analysis of masonry arch bridges interacting with the backfill. *Eng. Struct.*, **248**, 113189, 2021.

[10] G. Milani, P. B. Lourenço. 3D non-linear behavior of masonry arch bridges. *Comput. Struct.*, **110–111**, 133–150, 2012.

[11] M. Gilbert, D. Nguyen, C. Smith. Computational limit analysis of soil-arch interaction in masonry arch bridges. *Proc. 5th Int. Conf. arch Bridg. ARCH.* 633–640, 2007.

[12] R. K. Livesley. A computational model for the limit analysis of three-dimensional masonry structures. *Meccanica*, **27**, 161–172, 1992.

[13] M. Gilbert, C. Casapulla, H. M. Ahmed. Limit analysis of masonry block structures with non-associative frictional joints using linear programming. *Comput. Struct.*, **84**, 873–887, 2006.

[14] D. C. Drucker. Coulomb Friction, Plasticity, and Limit Loads. *J. Appl. Mech.*, **21**, 71–74, 1954.

[15] S. W. Sloan, P. W. Kleeman. Upper bound limit analysis using discontinuous velocity fields. *Comput. Methods Appl. Mech. Eng.*, **127**, 293–314, 1995.

[16] M. C. Ferris, F. Tin-Loi. Limit analysis of frictional block assemblies as a mathematical program with complementarity constraints. *Int. J. Mech. Sci.*, **43**, 209–224, 2001.

[17] D. Engwirda. Locally-optimal Delaunay-refinement and optimisation-based mesh generation, Ph.D. Thesis, School of Mathematics and Statistics, The University of Sydney, http://hdl.handle.net/2123/13148, 2014.

[18] Aaron T. Becker's Robot Swarm Lab. lloydsAlgorithm (Px, Py, crs, numIterations, showPlot) (https://www.mathworks.com/matlabcentral/fileexchange/41507-lloydsalgorithm-px-py-crs-numiterations-showplot), MATLAB Central File Exchange. Retrieved February 24, 2023.